Romanian Journal of Petroleum & Gas Technology
VOL. IV (LXXV) • No. 2/2023

HYDRODYNAMIC LOADS ON AN OFFSHORE WIND TURBINE IN THE ENVIRONMENTAL CONDITIONS OF THE BLACK SEA

Mariea Marcu

Petroleum-Gas University of Ploiesti, Romania
email: mmarcu@upg-ploiesti.ro

DOI: 10.51865/JPGT.2023.02.22

ABSTRACT

In the current context of promoting the large-scale use of renewable energy, the installation of wind turbines in the offshore and onshore environments is opportune. According to statistics, in 2022 offshore wind installations generated 21 GW, respectively 22.3% of a total of 94 GW produced by all offshore and onshore wind installations. This contribution was, also, estimated to increase in the coming years. In the Romanian sector of the Black Sea, the first wind farm will be installed in four years, according to the Romanian Ministry of Energy. Therefore, in our paper, we start with a short presentation of the different support types of the offshore wind turbine. According to the specialized literature, we found that the monopile has the simplest construction and is the most used in water with a depth of less than 50m. Further, we show theoretical aspects regarding the wave parameters and kinematics, wave spectra, wave forces, and overturning moments that act on a monopile in different conditions. Based on a Black Sea dataset and working scenarios, we performed several sensitivity studies on wind turbine support dimensions, wave characteristics, wave forces, and overturning moments. Finally, the variation ranges of wave forces and overturning moments will be estimated, under the environmental conditions of a Black Sea sector for different sizes of a monopile. These are useful in the design of an offshore wind turbine.

Keywords: wave force, wave spectra, offshore wind turbine, Black Sea

INTRODUCTION

In the current context of promoting the large-scale use of renewable energy, the installation of wind turbines in the offshore and onshore environments is opportune. In 2022, wind installations generated a total of 94 GW of which 21 GW were produced by those in the offshore environment [8]. This contribution is attempted to increase in the next years. The first wind farms in Romania's part of the Black Sea are expected in 2027-2028 [18].

Offshore wind turbines, compared to those installed onshore, are subject to more intense environmental conditions, because, in addition to the wind force, there are also the forces of waves and currents acting on the turbine support. Recently a lot of seasonal environmental parameters were measured in different areas of the Black Sea in order to establish if the wind farms are feasible in the Romanian sector of the Black Sea [12, 13]. The offshore wind turbines have different support types which depend on the water depth

as we show in the next section of the paper. From these, we choose the monopile because it is appropriate for water depth at the measurement points and also is a simple structure. Therefore, in our paper, we consider the environmental parameters to establish the magnitude of the wave forces and overturning moments that act on a monopile considering a regular, respectively irregular wave model.

TYPES OF WIND TURBINE

A wind turbine converts first the wind energy into mechanical energy. This mechanical energy activates a generator that produces electrical energy. The first wind turbine that generated electricity was installed in 1887 by James Blyth in Scotland [19]. Also in the same year, the American Charles Brush built the first automatic wind turbine [19].

Figure 1 shows several types of wind turbines. Some of these have blades with different configuration and orientation of the axis (horizontal plan (HAWT-Horizontal Axis Wind Turbine) or vertical plan (H-Blade VAWT- H-Blade Vertical Axis Wind Turbine)).

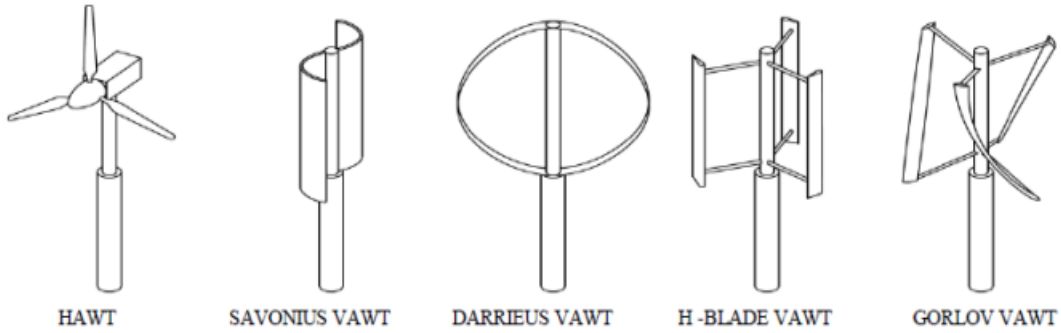

Figure 1. *Wind turbine with horizontal axis (HWAT) and vertical axis (*VAWT) [17].

The HAWT-type turbine with three blades is the most used [7, 19]. The wind turbines can be installed onshore and offshore environments. Compared to an onshore wind turbine, the one installed in the offshore environment requires a special support or substructure that constitutes the foundation of the wind turbine.

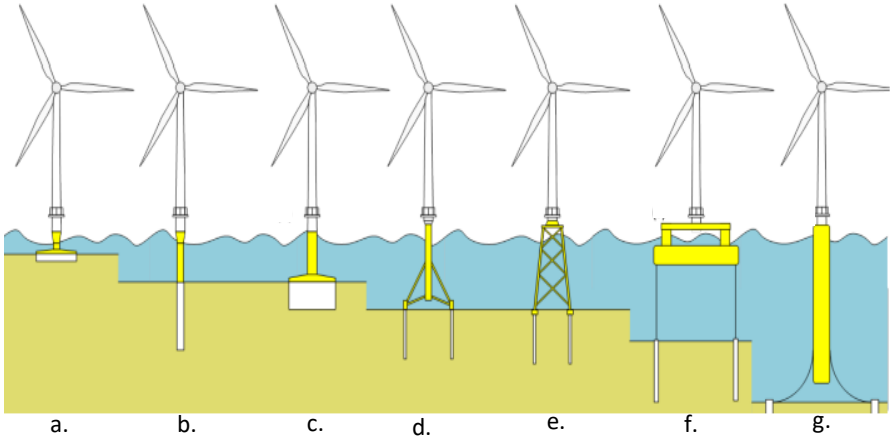

Figure 2. *Types of foundation for offshore wind turbines, a. gravity-base, b. monopole, c. suction caisson, d. tripod, e. jacket, f. TLP, g. ballast stabilized spar buoy* [1].

As can be seen from Figure 2, the substructure of the offshore wind turbine has different configurations being fixed or floating. The fixed substructures like monopile, tripod, jacket, gravity base, and suction caisson are used in relatively shallow waters. Alternatively, the floating structures (TLP and ballast stabilized spar buoy), are used in the deep water. All these substructures are subject to wave and current loads.

REGULAR AND IRREGULAR WAVES

Regular waves

The regular waves are the idealized having the same sinusoidal form on each cycle and the same characteristics for all cycles. In water of depth, d, regular waves are characterized by the following parameters: wavelength, L, period, T, angular frequency, ω, celerity, c, amplitude, a, number of wave, k, steepness, s (Figure 3).

Table 1 shows the regular wave parameters and their relations.

Table 1. *Waves parameters.*

Parameter	Measured unit	Equation
Angular frequency	rad/s	$\omega = 2\pi/T$ (1)
Wave amplitude	m	$a = H/2$ (2)
Celerity	m/s	$c = \sqrt{\frac{g}{k}\tanh(kd)}$ (3)
Wave number	-	$k = 2\pi/L$ (4)
Wave steepness	-	$s = \frac{H}{L}$ (5) if $s > 1/7$ wave too steep

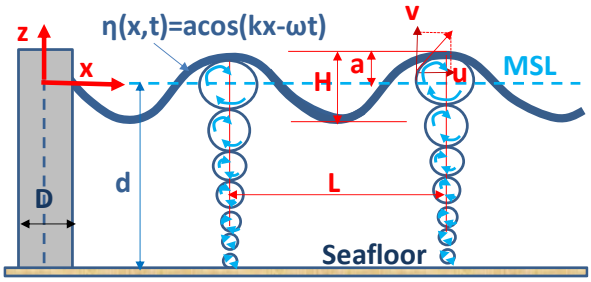

Figure 3. *Airy linear wave model.*

The free propagation of the waves with some amplitude, a occurs when the angular frequency, ω, and wave number, k satisfy the dispersion relationship [3]:

$$\omega^2 = gk\tanh(kd) \quad \text{or} \quad \frac{2\pi}{T^2} = \frac{g}{L}\tanh\left(\frac{2\pi d}{L}\right) \tag{6}$$

The wavelength, L, is calculated from the dispersion equation (6).

Using the product between wave number and water depth, kd or ratio between water depth and wavelength, d/L, the waves are [3, 6]:

- Deep water waves, for $kd > \pi$ or $d/L > 0.5$;
- Intermediate water waves, for $0.1\pi < kd < \pi$ or $0.05 < d/L < 0.5$;
- Shallow water waves, for $kd < 0.1\pi$ or $d/L \leq 0.05$.

In order to model the free surface of the sea and the wave kinematics in a deterministic manner, it was necessary to make the following assumptions [3, 10]: the fluid flow is ideal (without or little compressibility and without viscosity) and irrotational. Also, the flow is two-dimensional, the seabed is horizontal and the wave is regular with small steepness. The wave moves in the direction of the x-axis, the origin of the axes z-x is at the mean sea water level (MSL), and water particle velocities are smaller than wave celerity (Figure 3).

There are different wave theories like linear waves (Airy wave theory), the nth order Stokes theory, the cnoidal waves theory, the stream function theory, etc. [3, 5] to model the free surface and kinematics of the waves. Figure 4 shows a chart that allows the selection of wave theories taking into account the two ratios H/gT^2 and d/ gT^2.

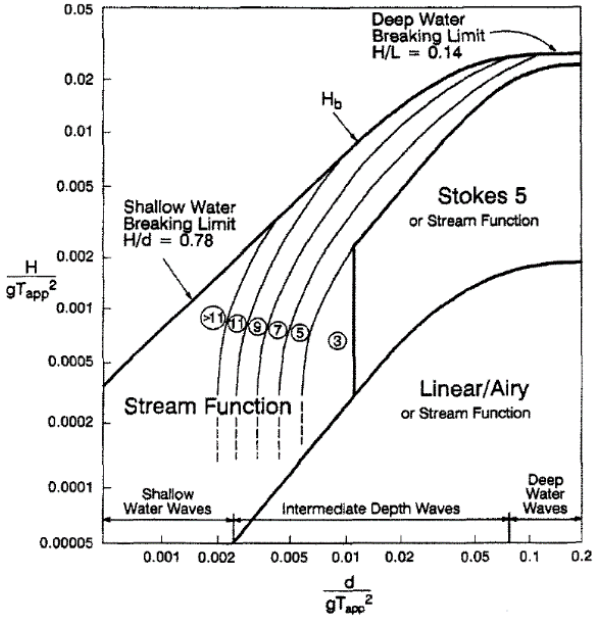

***Figure 4**. Chart for wave theory selection* [3].

The value of wave steepness, s is also used to decide between the linear or non-linear waves theory [5]. Therefore, the linear wave theory is chosen if s <0.01. Alternatively, for s >0.01 the 5th-order Stokes waves theory is more appropriate [4]. Because the application of 5th order Stokes wave theory is more complicated than linear wave theory, often the last one is used for waves with s >0.01 [5]. In the chart, the parameter H_b refers to the limit of wave height in a shallow and intermediate water depth.

Another way to select some wave theory is based on the product kH that can be calculated with the following equations [3]:

- For the superior limit of linear wave Airy theory:

$$kH = 0.8\frac{(\sinh(kd))^3}{(3+2(\sinh(kd))^2)\cosh(kd)} \tag{7}$$

- For a limit of linear wave Stokes 2nd order theory:

$$kH < 0.924\frac{(\sinh(kd))^3}{(1+8(\cosh(kd))^2)^{0.5}} \tag{8}$$

- For limit between 3rd and 5th order Stokes theories:
  - For shallow water

$$\frac{H}{d} < 0.725(kd)^2 \tag{9}$$

  - For deep water:

$$\frac{H}{d} < 0.1 \tag{10}$$

Also, the Ursell parameter or perturbation parameter that shows the influence of water depth on the non-linearity of waves given by the following relation [14]:

$$U_r = \frac{H}{d}\left(\frac{L}{d}\right)^2 \tag{11}$$

can be used to establish the wave theory in the case of shallow water, when the length of waves is larger than the water depth, $L \gg d$. Therefore, if the Ursell parameter is much smaller than 100, $U_r \ll 100$, linear wave theory can be considered.

Further, we consider the linear wave Airy theory and the 2nd order Strokes' theory because these are the most used and simplest. Also, we consider only the horizontal component of the velocity and acceleration of the water particles for the two theories (Table 2) because, in the calculus of wave force, only these components are necessary.

Table 2. *The free surface elevation and kinematics of the waves – Linear wave Airy theory and 2nd order Stokes theory.*

Parameter	**Linear Airy theory**	**2nd order Stokes theory**
Free surface elevation	$\eta(x,t) = a \cdot \cos(kx - \omega t)$ (12)	$\eta(x,t) = acos(kx - \omega t) + \frac{\pi}{2}\frac{a^2\, cosh(kd)}{L\, sinh^3(kd)} \cdot [2 + \cosh(2kd)]\cos(2(kx - \omega t))$ (13)
Velocity	$u(x,t) = \frac{a\omega \cdot \cosh(k(z+d))}{\sinh(kd)} \cdot \cos(kx - \omega t)$ (14)	$u(x,t) = \frac{2\pi a \cdot cosh(k(z+d))}{T\, sinh(kd)} \cdot cos(kx - \omega t) + \frac{3}{4c}\left(\frac{2\pi a}{T}\right)^2 \cdot \frac{cosh(2k(z+d))}{sinh^4(kd)} \cdot cos(2(kx - \omega t))$ (15) $c^2 = \frac{g}{k} tanh(kd)$ (16)
Acceleration	$\dot{u}(x,t) = \frac{\partial u(x,t)}{\partial t} = \frac{a\omega^2 \cdot \cosh(k(z+d))}{\sinh(kd)} \cdot \sin(kx - \omega t)$ (17)	$\dot{u}(x,t) = \frac{a\omega^2 \cdot \cosh(k(z+d))}{\sinh(kd)} \cdot \sin(kx - \omega t) + \frac{3\pi}{2L} \cdot \left(\frac{2\pi a}{T}\right)^2 \cdot \frac{\cosh(2k(z+d))}{(\sinh(kd))^4} \sin(2(kx - \omega t))$ (18)

In the table above:

a is the wave amplitude, m;

ω – wave angular frequency, rad/s;

$u(x,t)$ –horizontal component of wave velocity, m/s;

$\dot{u}(x,t)$ – horizontal component of wave acceleration, m/s^2;

t –time, s;

T – wave period, s;

H – wave height, $H = 2a$, m;

x, z –horizontal and vertical coordinate axes; $x = 0$ at the origin of the axis; $z = 0$ at mean water level, $z = -d$ at the seafloor and $z = \eta(x,t)$ at the instant water free surface elevation.

The parameters from Table 2 are determined along the wave at a level z.

Irregular waves

The sea waves are created by wind, ship movement, tides, or earthquakes having random characteristics, these being irregular waves (figure 5). The regular and unidirectional waves are very rare. Most often the sea waves are random with different heights, lengths, periods, and directions [6].

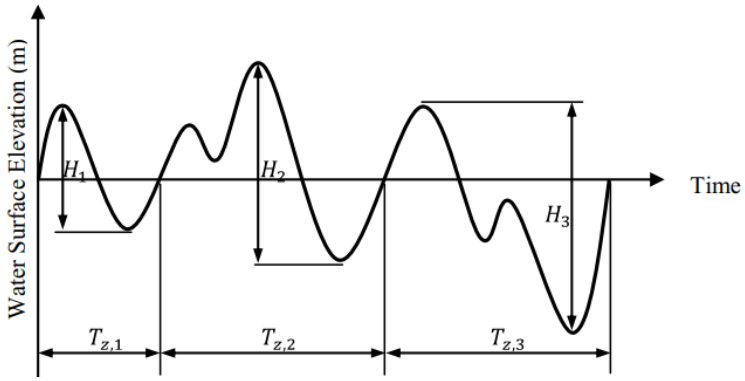

Figure 5. *Irregular waves and their parameters [10].*

These random waves can be considered as a sum of partial regular waves. In this case, the use of spectral analysis is appropriate to represent a random sea state. Therefore, the irregular wave can be described by statistical parameters like significant wave height, H_s, the highest wave height in the analyzed sample, H_{max}, mean wave height, H_{mean}, root mean square wave height, H_{rms}, mean of zero-crossing period, T_z, peak frequency, f, peak wave period, T_p, wave standard deviation, σ, 95th percentile H_s, 95th percentile T_p etc. The peak wave period or peak frequency is determined from the wave spectrum and corresponds to the wave with the highest energy.

The sea state depends on wind characteristics (speed, direction, and duration), water depth, and fetch. That is considered constant for a range of time at a location. Thus, the sea can be fully developed, developing, and non-fully developed [3]. The energy of the wind is transferred to the sea and the waves are formed. These random waves have different energy levels. The energy content in the waves is proportional to the squared displacement of the waves,η^2 [3, 10]. Using the Fast Fourier transform, the wave energy spectrum is obtained. That shows the distribution of the wave energy content over a frequency interval [10]. The most used models of spectral analysis are Pierson-Moskowitz and JONSWAP. The Pierson-Moskowitz model spectrum depends on a single

variable and describes a fully developed sea state, and the JONSWAP (Joint North Sea Wave Project*)* model depends on five variables and describes a non-fully developed sea state. These spectral models are used in the design of offshore structures [3, 10, 15].

In the paper, we use the Pierson-Moskowitz model spectrum, $S_{\eta\eta}(f)$, which is described by the following relation[3, 15]:

$$S_{\eta\eta}(f) = \frac{H_s^2}{4\pi f^5 T_z^4} \mathrm{e}^{-\frac{1}{\pi(fT_z)^4}} \tag{19}$$

where f is wave frequency, Hz;

$$f = \frac{\omega}{2\pi} = \frac{1}{T} \tag{20}$$

T_z −average mean zero-crossing wave period, s;

H_s −significant height, m;

$S_{\eta\eta}(f)$ − wave energy spectrum, m^2/Hz.

Thus, if the significant height of the wave and average mean-zero-crossing wave period are known we can recreate the energy history of an irregular wave [10]. The variance of the surface elevation, σ_η^2, by definition, is the area under the curve $S_{\eta\eta} = f(f)$:

$$\sigma_\eta^2 = \int_0^\infty S_{\eta\eta}(f)df \tag{21}$$

Another important parameter is the mean zero-upcrossing rate, ν_η which can be determined with the following relation [3]:

$$\nu_\eta = \sqrt{\frac{\int_0^\infty f^2 S_{\eta\eta}(f)\mathrm{d}f}{\int_0^\infty S_{\eta\eta}(f)\mathrm{d}f}} \tag{22}$$

WAVE FORCES AND OVERTURNING MOMENTS

Regular waves

We consider a monopile extended above the sea level and embedded in the seabed. To determine the wave force acting on a monopile of diameter, D, the Morison equation is used in the case of the slender cylinders with D/L<0.2, where L is the wavelength. According to Morison, the wave force, $dF(z,t)$, per unit height of a vertical cylinder with diameter, D is:

$$\mathrm{d}F(z,t) = dF_i(z,t) + dF_D(z,t) =$$
$$(\pi/4)C_M\rho D^2 \cdot \dot{u}(z,t) + 0.5C_D\rho D \cdot u(z,t)|u(z,t)| \tag{23}$$

where $F_i(t)$ and $F_D(t)$ are inertia and drag force, N;

C_M and C_D − inertia and drag coefficients;

ρ − sea water density, kg/m^3;

$u(z,t)$ − horizontal velocity of water particles, m/s;

D − vertical cylinder diameter, m.

As we observe from equation (23) the equation of Morison has two component related to the drag and inertia loads which depend on the velocity and acceleration of water particles.

If the eq.(23) is integrated between $z = -d$ and $z = 0$, it can be obtained the total wave force $F(t)$ [16]:

$$F(t) = \int_{-d}^{0} dF_i(z,t)dz + \int_{-d}^{0} dF_D(z,t)dz$$

$$F(t) = F_i(t) + F_D(t) = \frac{\pi^3 H}{2kT^2} C_M \rho D^2 \sin(kx - \omega t) + \frac{1}{8k} C_D \rho D \left(\frac{\pi H}{T}\right)^2 \frac{\sinh(2kd)+2kd}{(\sinh(kd))^2} \cdot \cos(kx - \omega t)|cos(kx - \omega t)| \quad (24)$$

Once the wave force is known, the overturning moment of the wind turbine monopile at the mudline level can be determined with the following equation [16]:

$$M(t) = \int_{-d}^{\eta} dF(z,t)(d+z)dz \quad (25)$$

According to Vugts et al [16], the maximum overturning moments can be determined with the following equation:

$$M_{max} = \rho g a d \frac{C_M \pi D^2}{4}\left[\tanh(kd) + \frac{1}{kd}\left(\frac{1}{\cosh(kd)} - 1\right)\right] + +\rho g \cdot \frac{C_D D}{2} a^2 \left[\frac{d}{2} + \frac{2(kd)^2+1-\cosh(2kd)}{4k \cdot \sinh(2kd)}\right] \quad (26)$$

Irregular waves

As we show above, a regular wave and linear wave theory, are easy to integrate, but for an irregular wave, the velocity is non-linear, and is difficult to determine an accurate response of the structure to the action of these waves.

Starting from the spectra of horizontal components of velocity and acceleration water particles which depend on wave spectrum $S_{\eta\eta}(f)$ and the complex transfer functions, the wave force spectrum, $S_{FF}(f)$ per unit length of a slender cylinder is given by the relation [2]:

$$S_{FF}(f) = S_{\eta\eta}(f)\left\{4\pi^2 f^2 \frac{[\cosh(kz)]^2}{[\sinh(kz)]^2}\left(\frac{8}{\pi} k_d^2 \sigma_u^2 + 4\pi^2 f^2 k_i^2\right)\right\} \quad (27)$$

where k_d, k_i are drag and inertia parameters given by the relations:

$$k_d = 0.5\rho C_D D; \quad k_i = 0.25\pi\rho C_M D^2 \quad (28)$$

$\sigma_u^2(z)$ – variance of the random velocity:

$$\sigma_u^2(z) = 2\int_0^{\infty} 4(\pi f)^2 \left[\frac{\cosh(kz)}{\sinh(kd)}\right]^2 S_{\eta\eta}(f)df \quad (29)$$

HYDRODYNAMIC LOADS ACTING ON A MONOPILE IN THE ROMANIAN SECTOR OF THE BLACK SEA

Environmental data

We consider a monopile installed in the Romanian sector of the Black Sea in the area identified as optimal for installing a wind farm [12, 13](Figure 6). In this area was performed several measurements to monitor the wind and wave parameters per each season (points 6, 7, and 8 from Figure 6). On the basis of these measurements, a lot of studies provide the wave and wind characteristics like significant wave height, H_s, peak period, T_p the wind velocity at 10 m above the sea level, $U_{10,}$ etc. (Table 3).

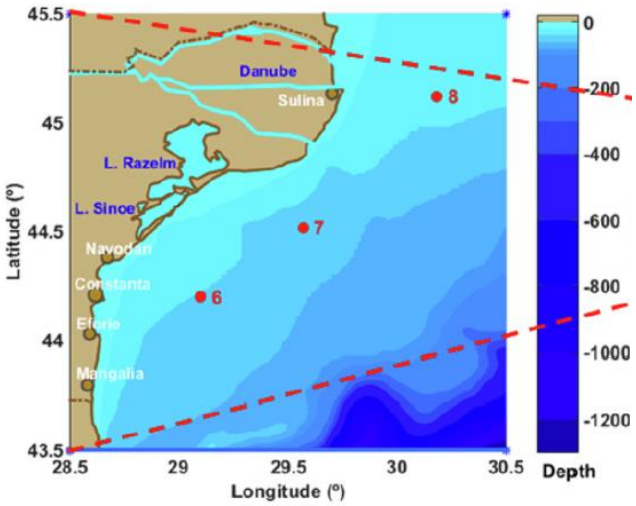

Figure 6. *Bathymetry of the Romanian sector of the Black Sea and the locations of points 6, 7, and 8* [14].

Table 3 shows the data regarding water depth, significant height, peak period of wave, wind speed, standard deviation, and 95th percentile of wind and wave parameters [13] at the locations of points 6, 7, and 8 from Figure 6.

Table 3*. Parameters of the waves and wind at the locations of the points 6, 7, and 8.*

Measurements points	M.U.	6	7	8	Mean values
Water depth, d	m	41	46	35	40.67
Mean H_s	m	0.88	0.89	0.90	0.89
Max H_s	m	7.06	7.10	6.94	7.03
StdvH_s	m	0.64	0.64	0.64	0.64
95th H_s	m	2.13	2.16	2.17	2.15
Mean T_p	s	4.54	4.62	4.44	4.53
Max T_p	s	13.19	12.64	12.89	12.91
StdvT_p	s	1.52	1.49	1.36	1.46
95th T_s	s	7.33	7.38	6.96	7.22
Mean U_{10}	m/s	6.34	6.38	6.49	6.40
Max U_{10}	m/s	24.75	24.39	24.02	24.39
Stdv,U_{10}	m/s	3.01	2.96	3.04	3.00
95th U_{10}	m/s	11.80	11.61	11.92	11.78

The density of Black Sea water in the superior strata is calculated with the relation of Millero and Poisson [11] taking into account the salinity (17g/l) [9]. Therefore, the resulting density is 1013 kg/m^3 at a temperature of 15^{o}C.

RESULT AND DISCUSSION

In our paper, we use the parameters of the waves shown in Table 3 to determine the kinematics of these and hydrodynamic loads that will act on a monopile in different working scenarios. Also, we consider regular and irregular waves.

Regular waves

We consider two working scenarios for regular waves which have the height and period shown in Table 4.

Table 4. *Working scenarios.*

Working scenario 1		**Working scenario 2**	
Mean H m	Mean T s	Max H m	Max T s
0.89	4.53	7.03	12.91

For each working scenario we calculate all the parameters of regular waves using the equations (1) through (11). The result of calculus is shown in table 5.

Table 5*. Parameters of the regular waves for the two working scenarios*

Parameters	**Working scenario 1**	**Working scenario 2**
Wave length, L, m	32.055	215.744
Angular frequency, ω rad/s	1.386	0.534
Wave amplitude, a, m	0.445	3.515
Celerity, c, m/s	7.076	16.711
Wave number, k	0.196	0.029
Wave steepness, s	0.028<1/7	0.033<1/7
kd	7.968 > π	0.1π < 1.183 < π
d/L	1.269 > 0.5	0.05 < 0.189 < 0.5
kH calculated	0.174	0.205
kH Airy theory limit	832873.706	0.628
kH 2nd order Stokes theory limit	680215.0384	0.582
Ursell parameter, U_r	0.014	4.771
Wave category	Deep water	Intermediate water

According to the criteria for establishing the water waves category, for the 1st working scenario, the water wave is deep because $kd > \pi$ and $\frac{d}{L} > 0.5$.

In the case of the 2nd working scenario water wave is intermediate because $0.1\pi < kd < \pi$ and $0.05 < \frac{d}{L} < 0.5$.

Comparing the calculated product kH with those which mark the limits of the theories application it results that for both working scenarios, the linear Airy wave theory and 2nd order Stokes wave theory are applicable. Also, from Table 5 we observe the wave steepness is low.

Further, we determine the variation of the free surface elevation and kinematics of the waves with the theories mentioned above (eqs. (12) through (18). The results of calculus are graphically shown in the figures below.

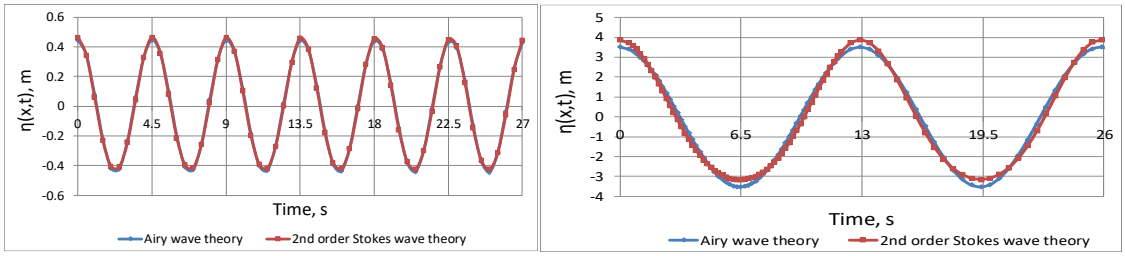

a. *b.*

Figure 7. *Variation of free waves surface.*
a. 1st working scenario for L=32m; b.2nd working scenario for L=216.3 m.

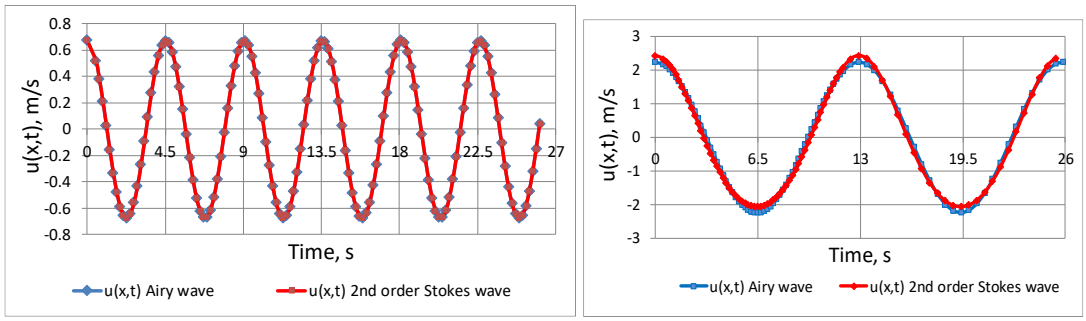

a. *b.*

Figure 8. *Variation of horizontal component of velocity*
a. 1st working scenario for z=0.44m; b.2nd working scenario for z=3.5 m.

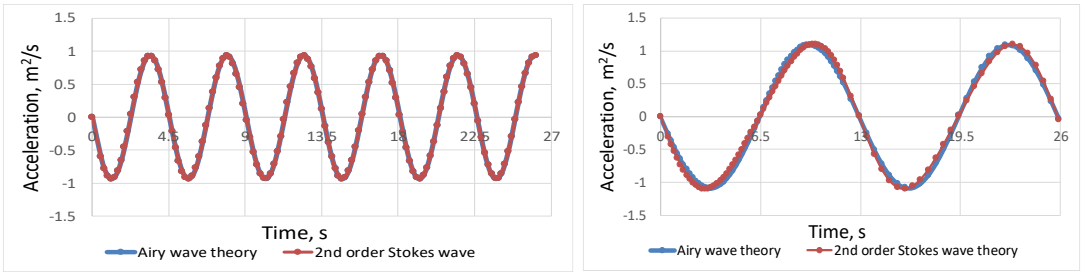

a. *b.*

Figure 9. *Variation of horizontal component of acceleration*
a. 1st working scenario for z=0.44m; b.2nd working scenario for z=3.5 m.

Figures 7 through 9 show that for the 1st working scenario which corresponds to deep water conditions, the variations with the time of the free surface elevation, horizontal velocity, and horizontal acceleration are the same indifferent to the used wave theory.

In the case of 2nd working scenario (for intermediate water wave), we observe a small difference between the results of the two theories for variation of free surface and horizontal velocity especially for minimum and maximum values of these parameters.

Also, in the case of the 2nd working scenario, for 2nd order Stokes theory, we observe an asymmetry between the crests (that become more sharps and higher) and troughs (that

become less sharp and more shallow) compared to the Airy linear wave theory (Figure 7b). Therefore, for the 2nd order Stokes theory, the maximum of $\eta(x,t) = 3.876$m and the minimum of $\eta(x,t) = -3.153$m, giving a wave height of 3.515 m that is the same with that obtained by the Airy linear wave theory.

As we observe from Figures 8 and 9, this difference between the results of the two theories is diminished in the case of the velocity and acceleration variations. Consequently, we consider that the linear wave theory of Airy in the case of the 2nd working scenario is appropriate.

Based on the linear Airy theory, we determine the variation of the wave force per unit height of a vertical cylinder with the time(eq.(23)) for both working scenarios mentioned above and consider two values of the monopile diameter like D_1 =6 m and D_2 = 8m.

Figures 10 and 11 show the variation of the inertia force, drag force, and total force for monopile diameter of 6m, respectively of 8m, and the two working scenarios.

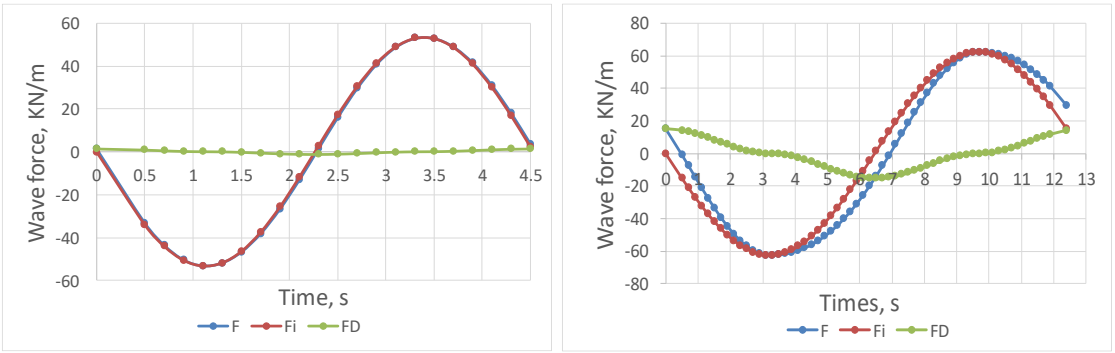

a. *b.*

Figure 10. *Variation of the inertia force, drag force, and total wave force per unit of length for D=6m; 1st working scenario (Hs=0.89 m, Tp=4.53 s); b.2nd working scenario (Hs=7.03 m, Tp=12.91 s)*

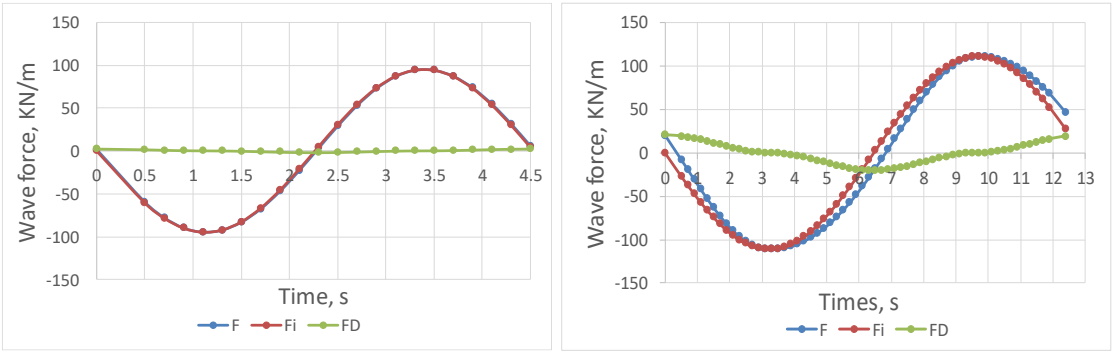

a. *b.*

Figure 11. *Variation of the inertia force, drag force, and total wave force per unit of length for D=8m; 1st working scenario (Hs=0.89 m, Tp=4.53 s); b.2nd working scenario (Hs=7.03 m, Tp=12.91 s)*

From the figures above, it results that in the case of the 1st working scenario the drag force, F_D is very small (negligible) compared with the inertia force, F_D.

In the 2nd working scenario, the drag force is also small, the total force being strongly influenced by the inertia force.

We use the relations (24) and (26) to determine the maximum of the wave's forces and the overturning moments, respectively in the case of the two working scenarios and two monopile diameters. The calculus results are shown in Table 6.

***Table 6**. Maximum wave force and overturning moment respectively*.

	$H = 0.89$m $T = 4.53$s	$H = 7.03$m $T = 12.91$s	$H = 0.89$m $T = 4.53$s	$H = 7.03$m $T = 12.91$s
	D_1 =6 m		D_1 =8 m	
F_{max}, kN	249.94	1638.656	444.34	2912.71
M_{max}, KNm	9150.21	45671.29	16148.13	77384.07

Table 6 shows that the increase of monopile diameter with 33% leads to approximately 77% increase in the total wave force. Also, when wave height and period increase, the wave forces increase by 6.5 times in our case indifferent of the value of monopile diameter.

The worst working scenario is the second for the monopile diameter of 8m. In this case, the total force and overturning moment have the highest values.

The maximum wave forces are registered at t=3.4 s for the first and t=9.8s for the second working scenario.

Irregular waves

In the case of irregular waves, we build the wave energy spectrum or wave spectral density ($S_{\eta\eta}(f)$) considering the Pierson-Moskovitz model (eq.(19)).

On the basis of the Pierson-Moskovitz model spectrum, we consider a limit for the wave frequency, f^* corresponding to the lowest level of the spectrum energy and we calculate the variance and standard deviation of the free surface elevation (eq.(21) and the mean zero-upcrossing rate (eq.(22)).

We consider also the two working scenarios shown in Table 4 and we build the wave energy spectra (Figure 12). Figures 12 a. and b. show a peak frequency of 0.223 Hz, respectively 0.077Hz.

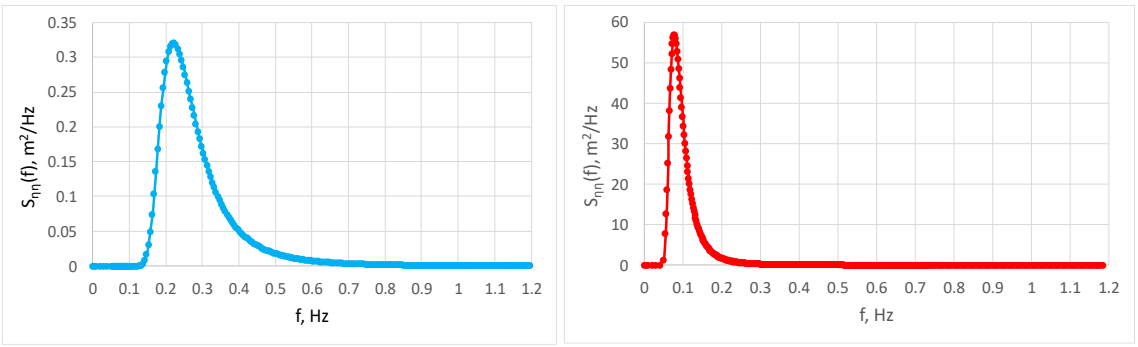

a. *b.*

***Figure 12.** Wave energy spectra for a. 1st working scenario (Hs=0.89 m, Tp=4.53 s); b.2nd working scenario (Hs=7.03 m, Tp=12.91 s)*

We set a frequency limit of 1.2 Hz because beyond this, the energy of the spectrum is negligible and the value of the standard deviation remains almost constant (Figure 13).

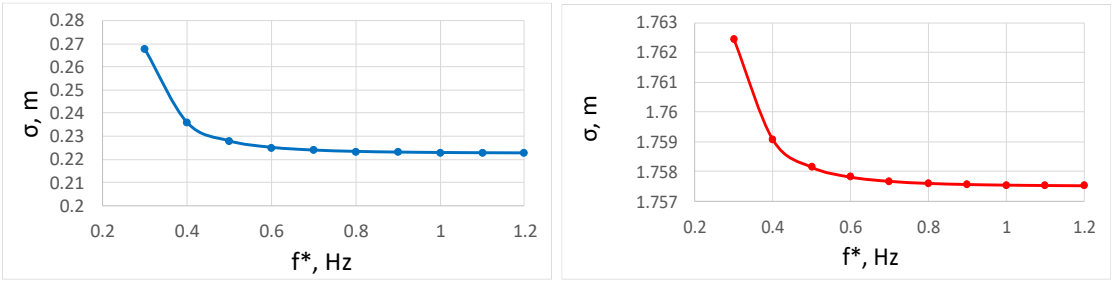

a. *b.*

Figure 13. *Variation of standard deviation with the limit of the frequency, f* for a. 1st working scenario; b.2nd working scenario.*

On the basis of the spectra from Figure 12, we determine the standard deviation of the surface elevation and the mean zero-upcrossing rate (eqs.(21) and (22)). Table 7 shows the calculus result for the two working scenarios.

Table 7*. Variance and standard deviation of surface elevation and mean zero-upcrossing rate.*

Working scenario 1 (Hs=0.89 m, Tp=4.53 s)			**Working scenario 2** (Hs=7.03 m, Tp=12.91 s)		
σ^2 m^2	σ m	ν_η Hz	σ^2 m^2	σ m	ν_η Hz
0.0495	0.222	0.311	3.088	1.757	0.109

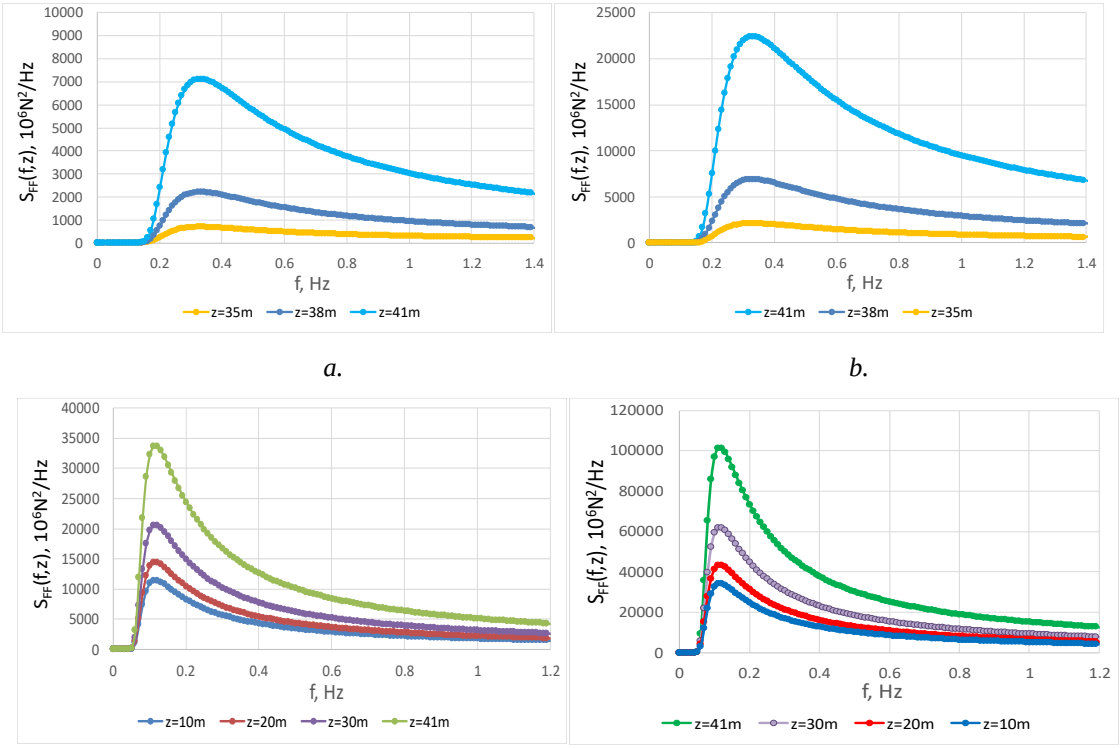

a. *b.*

c. *d.*

Figure 14. *Wave force spectra, $S_{FF}(f)$, for a. 1st working scenario, D=6m; b. 1st working scenario, D=8m; c. 2nd working scenario D=6m; d. 2nd working scenario, D=8m.*

Figure 14 shows that the maximum force of the waves that act on a monopile corresponds to a frequency of 0.331 Hz for the 1st working scenario and 0.121 Hz for the 2nd working scenario. As results from Figures 12 and 14, the peak frequency for the force spectrum is different than the peak frequency of the energy wave spectrum.

CONCLUSIONS

The goal of this paper was to estimate the wave kinematics, hydrodynamics loads, overturning moments, surface waves spectrum, and wave force spectrum in the case of a monopile which could be be installed in the Romanian sector of the Black Sea.

We consider also the regular and the irregular waves in two working scenarios (mean and maximum height and period) and also two values of monopile diameter to determine the wave forces and overturning moments.

In the case of the regular wave, we determine the appropriate wave theory for the two working scenarios. We consider Airy linear wave theory and 2nd order Stokes wave theory. Based on these, we calculate the variation of the free wave surface and the wave kinematics. From the comparison of the results provided by the two wave theories it results that for the first working scenario which correspond to the deep water wave, the two theory give approximately the same results. Alternatively, for the second working scenario, it registered little differences between the results of the two theories, especially in the case of the maximum and minimum values of parameters. Consequently, the Airy theory can be used also in the second working scenario.

The wave forces were determined for regular waves with the Morison equation. For both working scenarios, the drag force is much lower than the inertia force. Consequently, the total force is in fact equal to the inertia force. We determined the maximum wave forces and overturning moments and found that they increase significantly with increasing monopile diameter and environmental parameters. The wave forces and overturning moment are useful in the preliminary design of the monopile wind turbine. For irregular waves, we built the wave energy spectrum using the Pierson- Moskowitz model and we determined the variance, standard deviation, and mean zero-upcrossing rate. Also, we built the wave force spectra for both working scenarios and two monopile diameters. The peak frequency in these cases is different than the peak frequency of the energy wave spectrum.

REFERENCES

[1] Beuckelaers, W., Numerical Modelling of Laterally loaded Piles for Offshore wind turbine, Ph.D Thesis, Oxford, 2017

[2] Borgman, L.E. Spectral Analysis of Ocean Wave Forces on PiVmgs. Journal of the Waterways and Harbors Division, ASCE, WW2, Proc. Paper 5247, 1967, pp. 129-156.

[3] Chakrabarti, S., Handbook of offshore engineering, Vol.1, Elsevier, Amsterdam, 2005.

[4] Dean, R.G., Dalrymple, R., Water Wave Mechanics for Engineers and Scientists. World Scientific Publishing Ltd., Singapore, 1991.

[5] Folley, M., The Wave Energy Resource. In: Pecher, A., Kofoed, J. (eds) Handbook of Ocean Wave Energy. Ocean Engineering & Oceanography, vol 7. Springer, Cham. 2017

[6] Garrison, T., Essential of oceanography, 5th Edition, Brooks/Cole Cengage Learning, USA, 2009.

[7] Hau, E., Wind Turbines: Fundamentals, Technologies, Application, Economics, 2nd edition, Springer, 2006

[8] Lee, J, Zhao, F., Global Wind Report 2022, Global Wind Energy Council, 2022.

[9]Mihailov, M.E., Dinamica maselor de apa in Nord-Vestul Marii Negre, Ex Ponto, 2017

[10]Mohd Khair, A.H., Noor Irza, M.Z., Gholamhossein, N. Prediction of extreme offshore structural responses, LAP Lambert Academic Publishing, Germany, 2013.

[11] Millero F.J., Poisson, A., International one-atmosphere equation of state of seawater, Deep-Sea Research 28A (6) pp. 625–629, 1981.

[12] Rusu, L., Ganea, D., Mereuta, E., A joint evaluation of wave and wind energy resources in the Black Sea based on 20-year hindcast information, Energy Exploration & Exploitation, Vol.36(2) pp.335-351, 2018

[13] Rusu, L., The wave and wind power potential in the western Black Sea, Renewable Energy, 139, pp.1146-1158, 2019.

[14] Stansberg, C.T., Characteristics of steep second-order random waves in finite and shallow water. Proceedings of the ASME 2011 30th international conference on ocean, offshore and arctic engineering p. 859–69 Jan. 2011.

[15] Vist, H.T., Statistical properties of successive ocean wave parameters, Ph.D. Thesis, Trondheim, 2003.

[16] Vugts, J.H., van der Tempel, J., Schrama, E.A., Hydrodynamic loading on monotower support structures for preliminary design**,** Technical University Delft, 2001

[17] Zilberman, M., Sbaih, A.A., Hadad, I., Optimization of Small, Low Cost, Vertical Axis Wind Turbine for Private and Institutional Use, Conference ASME Gas Turbine India Conference, December 2021

[18] https://balkangreenenergynews.com, accessed October 2023.

[19] https://en.wikipedia.org/wiki/Wind_turbine, accessed October 2023.

Received: November 2023; Accepted: December 2023; Published: December 2023